International Journal of Advanced Robotic Systems

OPEN ACCESS
ARTICLE

Optimal Trajectory Planning and Coordinated Tracking Control Method of Tethered Space Robot Based on Velocity Impulse

Regular Paper

Panfeng Huang[1,2,*], Xiudong Xu[1,2] and Zhongjie Meng[1,2]

1 Research Center for Intelligent Robotics, School of Astronautics, Northwestern Polytechnical University, Xi'an, China
2 National Key Laboratory of Aerospace Flight Dynamics, Northwestern Polytechnical University, Xi'an, China
* Corresponding author E-mail: pfhuang@nwpu.edu.cn

Received 20 Aug 2013; Accepted 02 Jul 2014

DOI: 10.5772/58848

Abstract The tethered space robot (TSR) is a new concept of space robot which consists of a robot platform, space tether and operation robot. This paper presents a multi-objective optimal trajectory planning and a coordinated tracking control scheme for TSR based on velocity impulse in the approaching phase. Both total velocity impulse and flight time are included in this optimization. The non-dominated sorting genetic algorithm is employed to obtain the optimal trajectory Pareto solution using the TSR dynamic model and optimal trajectory planning model. The coordinated tracking control scheme utilizes optimal velocity impulse. Furthermore, the PID controller is designed in order to compensate for the distance measurement errors. The PID control force is optimized and distributed to thrusters and the space tether using a simulated annealing algorithm. The attitude interferential torque of the space tether is compensated a using time-delay algorithm through reaction wheels. The simulation results show that the multi-objective optimal trajectory planning method can reveal the relationships among flight time, fuel consumption, planar view angle and velocity impulse number. This method can provide a series of optimal trajectory according to a number of special tasks. The coordinated control scheme can significantly save thruster fuel for tracking the optimal trajectory, restrain the attitude interferential torque produced by space tether and maintain the relative attitude stability of the operation robot.

Keywords Tethered Space Robot, Velocity Impulse, Optimal Trajectory, Pareto Optimal Solutions, Coordinated Control, Time-delay

List of symbols

$\boldsymbol{F}_P$ /N net force of robot platform
$\boldsymbol{F}_R$ /N net force of operation robot
m_P /kg the mass of robot platform

m_R /kg the mass of operation robot
G / m^3 /$(\mathrm{kg}\cdot\mathrm{s}^2)$ universal gravitational constant
M_e / kg the mass of the earth
F_t tension force of space tether
$\boldsymbol{F}$ /N thruster force vector of operation robot
$\boldsymbol{r}_P$ /m position vector from O to P
$\boldsymbol{r}_R$ /m position vector from O to R
$\boldsymbol{r}_P^{o_1}$ /m position vector from O_1 to P
$\boldsymbol{r}_R^{o_1}$ /m position vector from O_1 to R
R_e /km orbital radius
l /m total releasing length of space tether
l_R /m tether length from R to O_1
l_P /m tether length from P to O_1
$\boldsymbol{r}_{o_1}$ /m position vector form O to O_1
Ω /rad/s orbital angular velocity
${}^{o_1}\boldsymbol{r}_P^R$ /m position vector from R to P
θ and ϕ /rad in-plane and out-of-plane angle of operation robot, respectively
a_x, a_y and a_z /m/s² thrust acceleration of operation robot
$\boldsymbol{X}=(x \quad y \quad z \quad \dot{x} \quad \dot{y} \quad \dot{z})^{\mathrm{T}}$ /m and m/s state vector
$\boldsymbol{U}=(0 \quad 0 \quad 0 \quad a_x \quad a_y \quad a_z)^{\mathrm{T}}$ /m/s² control vector
$\boldsymbol{A}$ and $\boldsymbol{B}$ state and control matrix, respectively
t_0 and t_f /s initial time and terminal time
$\boldsymbol{\Phi}_v$ velocity transfer matrix
$\boldsymbol{\Phi}_w$ position transfer matrix
$\boldsymbol{X}_0$ and $\boldsymbol{X}_f$ initial states and final states, respectively
M times of velocity impulse
δ /s time impulse
$\Delta\boldsymbol{V}$ /m/s velocity matrix
$\boldsymbol{\vartheta}$ arbitrary row vector suited to corresponding dimensions
$\boldsymbol{E}$ velocity transfer matrix of M velocity impulses
$\boldsymbol{E}^-$ Moore-Penrose inverse matrix of $\boldsymbol{E}$
$\boldsymbol{\omega}_c$ /rad/s angular velocity of operation robot
$\boldsymbol{Q}_r$ relative attitude quaternion of operation robot
$\boldsymbol{\omega}_r$ /rad/s relative angular velocity of operation robot
$\boldsymbol{\omega}_t$ /rad/s target angular velocity
$\boldsymbol{H}$ transformation matrix from the target orbit coordinate frame to the body coordinate frame
$\boldsymbol{I}^c$ / $\mathrm{kg}\cdot\mathrm{m}^2$ inertia matrix of operation robot
$\boldsymbol{J}^w$ / $\mathrm{kg}\cdot\mathrm{m}^2$ inertia matrix of reaction wheels
$\boldsymbol{\Omega}$ /rad/s angular velocity vector of reaction wheels
$\boldsymbol{h}_w$ angular momentum vector of reaction wheels
$\boldsymbol{h}_b$ angular momentum vector of operation robot
$\boldsymbol{T}_t$ / $\mathrm{N}\cdot\mathrm{m}$ interferential torque of space tether
$\boldsymbol{T}_w$ / $\mathrm{N}\cdot\mathrm{m}$ inertia axes' torque which the reaction wheels supply to the operation robot
$\boldsymbol{N}$ the input transformed matrix representing the influence on three inertia axes of each wheel
$\boldsymbol{U}_w$ / $\mathrm{N}\cdot\mathrm{m}$ input torque vector of four reaction wheels
$\boldsymbol{f}(\boldsymbol{x})$ optimal target function of trajectory planning model
$\boldsymbol{g}(\boldsymbol{x})$ constraint condition of trajectory planning model
Θ /rad maximum view angle
θ /rad real-time view angle measurement
$\boldsymbol{F}_t$ /N tension force vector after distributing control force
F_{xs}, F_{ys} and F_{zs} /N distribution control force of thrusters
J_f cost function of optimization and distribution control force
w_1 and w_2 weight coefficient
T_0 /℃ initial temperature
T_{min} /℃ minimum temperature
n iteration number
ξ annealing coefficient
$\boldsymbol{Y}$ / $\mathrm{N}\cdot\mathrm{m}$ attitude control compensation
$\hat{\boldsymbol{Y}}$ / $\mathrm{N}\cdot\mathrm{m}$ estimation of attitude control compensation
$\boldsymbol{\omega}_{rd}$ /rad/s desired relative angular velocity
$\boldsymbol{Q}_{rd}$ desired relative attitude quaternion
t_1 and t_2 /s time constant
T /s control period
l_x, l_y and l_z /m distance between connection point and centroid of operation robot

1. Introduction

With the development of space technology, the number of satellites increases dramatically. As many satellites are used together for a space mission, there have been some technical challenges. Some problems with satellites may emerge. Therefore, many researchers have studied problems of recycling and repair. The tethered space robot (TSR) is a new concept on-orbit mechanism for capturing the uncontrolled satellite, with potential applications for on-orbit maintenance, capture and assembly. This TSR consists of a robot platform, space tether and operation robot. The operation robot is released from the robot platform, attached by space tether; it then approaches the target automatically, finally capturing the uncontrolled satellite to accomplish on-orbit tasks. The TSR has a larger operation radius and better flexibility than a traditional space robot, because the combination of operation robot and space tether can be treated as an extended space arm.

Before the final task, the operation robot needs to arrive at the appropriate position with at a stable relative attitude. Therefore, the key technologies of this problem relate to optimal trajectory planning, tracking control and stability control of the relative attitude.

Generally, researchers have only considered fuel consumption in optimal trajectory planning. However, the approach time is also an important factor in the real task. Therefore, optimal trajectory planning of tethered

space robot needs to be further studied. In the traditional process of rendezvous, optimal trajectory planning is based on velocity impulse instead of continuous control force, because of the fuel limitations and thruster identity. The TSR has similar characteristics; however, when the approach distance is relatively short, the tension force of the space tether and the view angle should also be considered. Therefore, optimal trajectory planning of TSR has its own special aspects.

The optimized criteria include single objectives and multi-objectives for traditional optimal trajectory planning based on velocity impulse. Researchers often use genetic algorithms [4], ant colony algorithms [5] and simulated annealing. Luo et al. synthesized many optimized methods for designing an optimal long-distance trajectory based on velocity impulse, and considered the constraints of velocity [6]. Young and David optimized the rendezvous trajectory for two velocity impulses using a genetic algorithm whose variables are amplitude, imposed position and direction of velocity impulse. The optimal criterion is fuel consumption [7]. Zhang et al. proposed multi-objective (time and fuel consumption) optimal orbit transfer strategy using a genetic algorithm and Lambert's theory [8]. The existing studies, however, are dedicated to long- distance rendezvous trajectory, and thus are different from the optimal trajectory planning of a tethered space robot. This paper presents optimal trajectory planning for approaching the target based on velocity impulse, and includes consideration for the final approach and capture task.

The fuel consumption is a major consideration for tracking the optimal trajectory of TSR. To save the fuel of the operation robot, this paper presents a coordinated orbit and attitude control method for tracking the optimal trajectory. For coordinated control, Nakamura et al. discussed the collaborative control of tension force (controlled by the service satellite) and thruster force (controlled by tethered robot) for approaching the target of the tethered retriever, but did not consider attitude [9]. Nohmi designed a tethered space robot, connected to a mother spacecraft through space tether. The attitude of the tethered subsystem can be controlled by tether tension force through its own link motion, and the tethered subsystem rotates when its mass centre deviates from equilibrium, which is controlled by the arm [10]. He also developed a space robot attached to a spacecraft by tether. The spacecraft-mounted manipulator generated the necessary initial momentum for the space robot and adjusted its trajectory by controlling tether tension [11]. Mori proposed the concept of tethered satellite cluster systems whose parts were connected by tethers. He established a coordinated control method using tension force and thrust force, which decreased thruster fuel and improved control precision [12]. A coordinated fault-tolerant nonlinear control method was presented by Godard [13] to control the attitude of a satellite using movement of tether attachment points; his method examined cases where tether deployment suddenly stops and tether breakage occurs. Chang et al. proposed an adaptive coordinated control strategy for a robot system which can control its own movement [14]. The TSR is similar in concept to the above researches, which mention the coordinated control method; however, they only considered one aspect, such as orbit movement or attitude change.

The attitude control problem is a complex topic due to the nonlinear nature of the model, coupled with uncertainties both in parameters and disturbances [15, 16]. Many attitude control methods are available, including linear and nonlinear H∞ [17, 18], adaptive control [19] and fuzzy controls [20, 21]. The reaction wheel has become increasingly popular as an actuator in spacecraft attitude control [22]. Kristiansen discussed the advantages of this type [22]. The reaction wheel is a device that applies torque to spacecraft by control command. Ismail presented several configurations of reaction wheels and the standard reaction wheel control, and angular momentum unloading schemes were adopted for all configurations of the reaction wheel [23]. Jin proposed a simple and effective fault tolerant control method for satellites with four wheels. This method was based on dynamic inversion and time-delay control theory [24].

This paper presents an optimal trajectory of an operation robot for approaching the target based on the multi-objective velocity impulse method. To economize the thrust fuel of operation robot, we present a coordinated orbit control and attitude stability method for tracking the optimal approach trajectory. The rest of the paper is organized as follows: first, a brief description of the tethered space robot is given. Next, the TSR dynamic model is presented in Section II. Then, the optimal trajectory model of the operation robot is introduced for approaching the target based on velocity impulse in Section III. Furthermore, the coordinated orbit control and attitude stability method are detailed for tracking the optimal trajectory in Section IV. Finally, the numerical results of the optimal trajectory and the coordinated control method are plotted in Section V, and conclusions are given at the end.

2. TSR Task Description

This paper proposes a TSR system composed of a robot platform, space tether and operation robot, whose task is on-orbit service. An operation robot is the machine to perform this work. The task flow is described as follows. The operation robot is installed at the robot platform in the initial state. The TSR approaches the position close to 100 metres' distance and level with the target under the guidance, navigation and control of its own equipment.

Then, the operation robot approaches the target after being released from the robot platform, maintaining its relative attitude according to the target attitude. Finally, the operation robot supplies on-orbit service using its own manipulator after reaching the appointed position (<1 m to the target). The TSR is shown in Figure 1.

This paper firstly studies optimal trajectory planning in approaching the target of the operation robot, which is released by the robot platform by space tether. Then, it provides a coordinated orbit control and attitude stability method for tracking optimal trajectory. The actuators of the operational robot are thrusters and reaction wheels. The thrusters consume the fuel of the operation robot, while the reaction wheels consume electricity from the robot platform through space tether. To save the fuel of the operation robot, this article studies coordinated orbit control using space tether and thrusters, maintaining the relative attitude using reaction wheels.

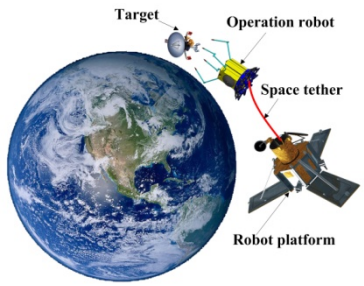

Figure 1. Tethered space robot construction

3. Operation Robot Dynamic Model for Approaching the Target

3.1 Operation Robot Orbital Dynamic Model

First, the dynamic model of TSR is established. The mass of space tether is ignored; the robot platform and operation robot are modelled as two mass points when we establish the orbital dynamic model of the operation robot, which are represented as symbol R and P in circular orbit. The o_1 is the centroid of TSR, the $o_1x_1y_1z_1$ frame is the TSR orbit coordinate frame and the $o_1x_2y_2z_2$ frame is the coordinate frame of space tether. The in-plane and out-of-plane angles are θ and ϕ, respectively. All of these are shown in Figure 2.

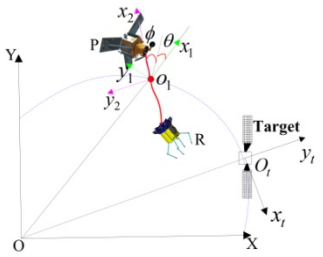

Figure 2. Relevant coordinate frame of TSR

The following dynamic equation of TSR is obtained by Newton's Second Law:

$$\frac{\boldsymbol{F}_P}{m_P}-\frac{\boldsymbol{F}_R}{m_R}=\left(\frac{-GM_e}{|\boldsymbol{r}_P|^2}\frac{\boldsymbol{r}_P}{|\boldsymbol{r}_P|}-\frac{F_t}{m_P}\frac{\boldsymbol{r}_P^{o_1}}{|\boldsymbol{r}_P^{o_1}|}\right)-\left(\frac{-GM_e}{|\boldsymbol{r}_R|^2}\frac{\boldsymbol{r}_R}{|\boldsymbol{r}_R|}-\frac{F_t}{m_R}\frac{\boldsymbol{r}_R^{o_1}}{|\boldsymbol{r}_R^{o_1}|}+\frac{\boldsymbol{F}}{m_R}\right) \tag{1}$$

where $\boldsymbol{F}_P$ and $\boldsymbol{F}_R$ are the net force acting on the robot platform and operation robot, and m_P and m_R are the mass of the two bodies, respectively. $G=6.67\times10^{-11}\mathrm{m}^3/(\mathrm{kg}\cdot\mathrm{s}^2)$ is the universal gravitational constant. $M_e=5.98\times10^{24}\mathrm{kg}$ is the mass of the earth. F_t is the tension force of space tether. $\boldsymbol{F}=[F_1,F_2,F_3]^{\mathrm{T}}$ is the thruster force of the operation robot in $o_1x_2y_2z_2$ coordinate frame. $\boldsymbol{r}_P$ and $\boldsymbol{r}_R$ are the position vectors from the O to the end-body P and R. $\boldsymbol{r}_P^{o_1}$ and $\boldsymbol{r}_R^{o_1}$ are the position vectors from the O_1 to P and R.

It is assumed that R_e is the orbital radius, l is the total releasing length of space tether, l_R is tether length from R to O_1, and l_P is the tether length from P to O_1. Therefore, the position vectors $\boldsymbol{r}_P$ and $\boldsymbol{r}_R$ can be expressed in the frame $o_1x_2y_2z_2$ as:

$$\boldsymbol{r}_P=\boldsymbol{r}_{o_1}+\boldsymbol{r}_P^{o_1}=\begin{bmatrix}l_P+R_e\cos\theta\cos\phi\\-R_e\sin\theta\\-R_e\cos\theta\sin\phi\end{bmatrix} \tag{2}$$

$$\boldsymbol{r}_R=\boldsymbol{r}_{o_1}+\boldsymbol{r}_R^{o_1}=\begin{bmatrix}-l_R+R_e\cos\theta\cos\phi\\-R_e\sin\theta\\-R_e\cos\theta\sin\phi\end{bmatrix} \tag{3}$$

where $\boldsymbol{r}_{o_1}$ is the position vector from O to o_1. The following equations are easily obtained:

$$|\boldsymbol{r}_P|^{-3}\approx\frac{1}{R_e^3}\left(1-3\frac{l_P}{R_e}\cos\theta\cos\phi\right) \tag{4}$$

$$|\boldsymbol{r}_R|^{-3}\approx\frac{1}{R_e^3}\left(1+3\frac{l_R}{R_e}\cos\theta\cos\phi\right) \tag{5}$$

Substituting all the terms on the right hand side of Eq. (1) with the equations above and simplifying yields:

$$\frac{\boldsymbol{F}_P}{m_P}-\frac{\boldsymbol{F}_R}{m_R}=\begin{bmatrix}-\Omega^2l+3\Omega^2l\cos^2\theta\cos^2\phi-\dfrac{F_t(m_P+m_R)}{m_P\cdot m_R}-F_1\\-3\Omega^2l\cos\theta\sin\theta\cos\phi-F_2\\-3\Omega^2l\cos^2\theta\cos\phi\sin\phi-F_3\end{bmatrix} \tag{6}$$

where $\Omega = \sqrt{GM_e / R_e^3}$.

The relative angular velocity $\boldsymbol{\omega}_O^{o_1}$ and angular acceleration $\boldsymbol{\alpha}_O^{o_1}$ between the inertial frame $OXYZ$ and $o_1x_2y_2z_2$ frame can be expressed in the frame $o_1x_2y_2z_2$:

$$\boldsymbol{\omega}_O^{o_1} = \begin{bmatrix} (\dot{\theta}+\Omega)\sin\phi \\ -\dot{\phi} \\ (\dot{\theta}+\Omega)\cos\phi \end{bmatrix}, \boldsymbol{\alpha}_O^{o_1} = \begin{bmatrix} \ddot{\theta}\sin\phi + (\dot{\theta}+\Omega)\dot{\phi}\cos\phi \\ -\ddot{\phi} \\ \ddot{\theta}\cos\phi - (\dot{\theta}+\Omega)\dot{\phi}\sin\phi \end{bmatrix} \quad (7)$$

The ${}^{o_1}\boldsymbol{r}_P^R$ is position vector from R to P , and its derivatives are differentiated in the $o_1x_2y_2z_2$ frame, as can be expressed as:

$${}^{o_1}\boldsymbol{r}_P^R = \begin{bmatrix} l \\ 0 \\ 0 \end{bmatrix}, {}^{o_1}\dot{\boldsymbol{r}}_P^R = \begin{bmatrix} \dot{l} \\ 0 \\ 0 \end{bmatrix}, {}^{o_1}\ddot{\boldsymbol{r}}_P^R = \begin{bmatrix} \ddot{l} \\ 0 \\ 0 \end{bmatrix} \quad (8)$$

Therefore, the inertial acceleration $\ddot{\boldsymbol{r}}_P^R$ can be expressed as:

$$\ddot{\boldsymbol{r}}_P^R = {}^{o_1}\ddot{\boldsymbol{r}}_P^R + \boldsymbol{\alpha}_O^{o_1} \times \boldsymbol{r}_P^R + 2\boldsymbol{\omega}_O^{o_1} \times {}^{o_1}\dot{\boldsymbol{r}}_P^R + \boldsymbol{\omega}_O^{o_1} \times (\boldsymbol{\omega}_O^{o_1} \times \boldsymbol{r}_P^R) \quad (9)$$

Substituting all the terms on the right hand side of Eq. (9) with the Eqs. (7) and (8), and simplifying, we obtain:

$$\ddot{\boldsymbol{r}}_P^R = \begin{bmatrix} \ddot{l} - \dot{\phi}^2 l - (\dot{\theta}+\Omega)\cos^2\phi l \\ \ddot{\theta}\cos\phi l - 2(\dot{\theta}+\Omega)\dot{\phi}\sin\phi l + 2(\dot{\theta}+\Omega)\cos\phi\dot{l} \\ \ddot{\phi} l + 2\dot{\phi}\dot{l} + (\dot{\theta}+\Omega)^2\cos\phi\sin\phi l \end{bmatrix} \quad (10)$$

The Eqs. (6) and (10) can be set equal to each other to obtain dynamic model of TSR:

$$\begin{aligned} \ddot{l} &= \dot{\phi}^2 l + (\dot{\theta}+\Omega)^2\cos^2\phi l - \Omega^2 l + 3\Omega^2 l\cos^2\theta\cos^2\phi - F_t\frac{m_p + m_R}{m_p \cdot m_R} - F_1 \\ \ddot{\theta} &= 2(\dot{\theta}+\Omega)\dot{\phi}\tan\phi - 2(\dot{\theta}+\Omega)\frac{\dot{l}}{l} - 3\Omega^2\cos\theta\sin\theta - F_2 \\ \ddot{\phi} &= -2\dot{\phi}\frac{\dot{l}}{l} - (\dot{\theta}+\Omega)^2\cos\phi\sin\phi - 3\Omega^2\cos^2\theta\cos\phi\sin\phi - F_3 \end{aligned} \quad (11)$$

Generally, the mass of the robot platform is larger than that of the operation robot; furthermore, the mass of the space tether is ignored. Therefore, the centroid of TSR can be almost considered as the centroid of the robot platform. In this paper, we assume that the target is located in the same circular orbit as the TSR and the releasing length of the space tether is 100 metres level. The relative motion of the operation robot can be described by a Hill equation in the target orbit coordinate frame $o_tx_ty_tz_t$, as shown in Figure 1.

$$\begin{cases} \ddot{x} - 2\Omega\dot{y} = a_x \\ \ddot{y} + 2\Omega\dot{x} - 3\Omega^2 y = a_y \\ \ddot{z} + \Omega^2 z = a_z \end{cases} \quad (12)$$

where a_x , a_y and a_z are the thrust acceleration of the operation robot. Denoting the state vector $\boldsymbol{X} = (x \quad y \quad z \quad \dot{x} \quad \dot{y} \quad \dot{z})^{\mathrm{T}}$ and the control vector $\boldsymbol{U} = (0 \quad 0 \quad 0 \quad a_x \quad a_y \quad a_z)^{\mathrm{T}}$, Eq. (12) is revised as follows:

$$\dot{\boldsymbol{X}} = \boldsymbol{A}\boldsymbol{X} + \boldsymbol{B}\boldsymbol{U} \quad (13)$$

where $\boldsymbol{A} = \begin{pmatrix} 0 & 0 & 0 & 1 & 0 & 0 \\ 0 & 0 & 0 & 0 & 1 & 0 \\ 0 & 0 & 0 & 0 & 0 & 1 \\ 0 & 0 & 0 & 0 & 2\Omega & 0 \\ 0 & 3\Omega^2 & 0 & -2\Omega & 0 & 0 \\ 0 & 0 & -\Omega^2 & 0 & 0 & 0 \end{pmatrix}$, $\boldsymbol{B} = \begin{pmatrix} 0 & 0 & 0 \\ 0 & 0 & 0 \\ 0 & 0 & 0 \\ 1 & 0 & 0 \\ 0 & 1 & 0 \\ 0 & 0 & 1 \end{pmatrix}$.

From Eq. (13), the state transition matrix is obtained:

$$\boldsymbol{\Phi}(t, t_0) = \begin{pmatrix} 1 & 6(\tau - \sin\tau) & 0 & \frac{4\sin\tau - 3\tau}{\Omega} & \frac{2(1-\cos\tau)}{\Omega} & 0 \\ 0 & 4 - 3\cos\tau & 0 & \frac{-2(1-\cos\tau)}{\Omega} & \frac{\sin\tau}{\Omega} & 0 \\ 0 & 0 & \cos\tau & 0 & 0 & \frac{\sin\tau}{\Omega} \\ 0 & 6\Omega(1-\cos\tau) & 0 & 4\cos\tau - 3 & 2\sin\tau & 0 \\ 0 & 3\Omega\sin\tau & 0 & -2\sin\tau & \cos\tau & 0 \\ 0 & 0 & -\Omega\sin\tau & 0 & 0 & \cos\tau \end{pmatrix} \quad (14)$$

where $\tau = \Omega(t - t_0)$. From Eq. (13), we get its special solution satisfying $\boldsymbol{X}(t_0) = \boldsymbol{X}_0$:

$$\boldsymbol{X}(t) = \boldsymbol{\Phi}(t, t_0)\boldsymbol{X}_0 + \int_{t_0}^{t} \boldsymbol{\Phi}_v(t, s)\boldsymbol{U}(s)\mathrm{d}s \quad (15)$$

where $\boldsymbol{\Phi}_v$ is velocity transfer matrix. Eq. (14) can be rewritten as:

$$\boldsymbol{\Phi}(t, t_0) = \begin{pmatrix} \boldsymbol{\Phi}_{11} & \boldsymbol{\Phi}_{12} \\ \boldsymbol{\Phi}_{21} & \boldsymbol{\Phi}_{22} \end{pmatrix} \quad (16)$$

Eq. (16) can be rewritten as:

$$\boldsymbol{\Phi}(t, t_0) = \boldsymbol{\Phi}_w(t, t_0) + \boldsymbol{\Phi}_v(t, t_0) \quad (17)$$

where $\boldsymbol{\Phi}_w(t, t_0) = \begin{bmatrix} \boldsymbol{\Phi}_{11} \\ \boldsymbol{\Phi}_{21} \end{bmatrix}$ is position transfer matrix, and $\boldsymbol{\Phi}_v(t, t_0) = \begin{bmatrix} \boldsymbol{\Phi}_{12} \\ \boldsymbol{\Phi}_{22} \end{bmatrix}$ is velocity transfer matrix.

It is assumed that $\boldsymbol{X}_0$ is initial states, $\boldsymbol{X}_f$ is final states, t_0 is the initial time and t_f is the final time. The operation robot can have M velocity impulses imposed; therefore, the control vector $\boldsymbol{U}_r$ can be illustrated as:

$$\boldsymbol{U}_r(t) = \sum_{i=1}^{M} \Delta \boldsymbol{v}_i \delta(t - t_i) \tag{18}$$

where t_i is the time in which the velocity impulse is imposed, $\Delta \boldsymbol{v}_i = (\Delta v_{xi} \quad \Delta v_{yi} \quad \Delta v_{zi})^{\mathrm{T}}$. Substituting Eq. (18) into Eq. (15), Eq. (19) can be obtained:

$$\boldsymbol{X}(t_f) = \boldsymbol{\Phi}(t, t_0)\boldsymbol{X}_0 + \sum_{i=1}^{M} \boldsymbol{\Phi}_v(t_f, t_i)\Delta \boldsymbol{v}_i \tag{19}$$

Eq. (19) can be rewritten as:

$$\boldsymbol{X}(t) - \boldsymbol{\Phi}(t, t_0)\boldsymbol{X}_0 = \boldsymbol{E}\Delta \boldsymbol{V} \tag{20}$$

where $\boldsymbol{E} = \left[\boldsymbol{\Phi}_v(t_f, t_2) \quad \boldsymbol{\Phi}_v(t_f, t_1) \quad \cdots \quad \boldsymbol{\Phi}_v(t_f, t_M)\right]$,

$\Delta \boldsymbol{V} = \left[(\Delta \boldsymbol{v}_1)^{\mathrm{T}} \quad (\Delta \boldsymbol{v}_2)^{\mathrm{T}} \quad \cdots \quad (\Delta \boldsymbol{v}_M)^{\mathrm{T}}\right]^{\mathrm{T}}$.

When two velocity impulses are imposed on the operation robot, it can be calculated by Eq. (20):

$$\Delta \boldsymbol{V} = \boldsymbol{E}^{-1}(\boldsymbol{X}(t) - \boldsymbol{\Phi}(t, t_0)\boldsymbol{X}_0) \tag{21}$$

When three (> three) velocity impulses are imposed, the general solution of M velocity impulses can be obtained by Eq. (20):

$$\Delta \boldsymbol{V} = \boldsymbol{E}^{-}(\boldsymbol{X}(t) - \boldsymbol{\Phi}(t, t_0)\boldsymbol{X}_0) + (\mathrm{I} - \boldsymbol{E}^{-}\boldsymbol{E})\boldsymbol{\vartheta} \tag{22}$$

where $\boldsymbol{\vartheta}$ is an arbitrary row vector suited to the corresponding dimensions. If the minimum-norm solution is chosen, Eq. (22) can be rewritten as:

$$\Delta \boldsymbol{V} = \boldsymbol{E}^{-}(\boldsymbol{X}(t) - \boldsymbol{\Phi}(t, t_0)\boldsymbol{X}_0) \tag{23}$$

$\boldsymbol{E}^{-} = \boldsymbol{E}^{\mathrm{T}}(\boldsymbol{E}\boldsymbol{E}^{\mathrm{T}})^{-1}$ is the Moore-Penrose inverse matrix in Eqs. (22) and (23). However, the minimum-norm solution is different from the minimum-fuel solution. The minimum-fuel solution can be obtained through seeking optimal arbitrary row vector $\boldsymbol{\vartheta}$ with the minimum-norm solution $\Delta \boldsymbol{V}$ as the initial guess.

3.2 Attitude Kinematic and Dynamic Model of the Operation Robot

This paper focuses on the coordinated relative attitude control and stability of the operation robot for approaching the target, so it is defined that $\boldsymbol{\omega}_c = [\omega_{cx} \quad \omega_{cy} \quad \omega_{cz}]^{\mathrm{T}}$ is the angular velocity vector of the operational robot. The relative attitude kinematic equation of the operation robot is established using attitude quaternion in this paper. The paper also defines $\boldsymbol{q}_r = [q_1 \quad q_2 \quad q_3]^{\mathrm{T}}$ and $\boldsymbol{Q}_r = [q_0 \quad \boldsymbol{q}_r{}^{\mathrm{T}}]^{\mathrm{T}}$, which satisfy $q_0^2 + q_1^2 + q_2^2 + q_3^2 = 1$. $\boldsymbol{Q}_r$ is the relative attitude quaternion of the operation robot. It is defined as $\boldsymbol{Q}_r^{\times} = \begin{bmatrix} -q_1 & -q_2 & -q_3 \\ q_0 & -q_3 & q_2 \\ q_3 & q_0 & -q_1 \\ -q_2 & q_1 & q_0 \end{bmatrix}$.

Thus, the relative attitude quaternion kinematic equation is obtained by:

$$\dot{\boldsymbol{Q}}_r = \frac{1}{2}\boldsymbol{Q}_r^{\times}\boldsymbol{\omega}_r \tag{24}$$

where $\boldsymbol{\omega}_r$ is rotation angular velocity of operation robot relative to the target. The operation robot is provided with four reaction wheels, where three are installed by three inertia axes and the fourth is installed in the position at the same angle as the other three.

From the relative attitude relationship, it is concluded that:

$$\boldsymbol{\omega}_r = \boldsymbol{\omega}_c - \boldsymbol{H}\boldsymbol{\omega}_t \tag{25}$$

where $\boldsymbol{\omega}_t$ is target angular velocity, $\boldsymbol{H}$ is the transformed matrix from target orbit coordinate frame to body coordinate frame of operation robot.

$$\boldsymbol{H} = \begin{bmatrix} q_0^2 + q_1^2 - q_2^2 - q_3^2 & 2q_0q_3 + 2q_1q_2 & -2q_0q_2 + 2q_1q_3 \\ -2q_0q_3 + 2q_1q_2 & q_0^2 - q_1^2 + q_2^2 - q_3^2 & 2q_0q_1 + 2q_2q_3 \\ 2q_0q_2 + 2q_1q_3 & -2q_0q_1 + 2q_2q_3 & q_0^2 - q_1^2 - q_2^2 + q_3^2 \end{bmatrix}$$

Assume: $\boldsymbol{I}^c = \mathrm{diag}(I_x^c, I_y^c, I_z^c)$ is inertia matrix of the operation robot, $\boldsymbol{J}^w = \mathrm{diag}(J_1^w, J_2^w, J_3^w, J_4^w)$ is inertia matrix of reaction wheels, $\boldsymbol{\Omega} = [\Omega_1 \quad \Omega_2 \quad \Omega_3 \quad \Omega_4]^{\mathrm{T}}$ is the angular velocity of reaction wheels relative to the operation robot, $\boldsymbol{h}_w$ is the angular momentum vector of the reaction wheels, $\boldsymbol{h}_b$ is the angular momentum vector of the operation robot, $\boldsymbol{T}_t$ is the tether interferential torque of the operation robot, $\boldsymbol{T}_w$ is the inertia axes' torque which the reaction wheels supply to the operation robot, $\boldsymbol{N}$ is the input transformed matrix representing the influence on the three inertia axes of each wheel, and $\boldsymbol{U}_w = [u_1 \quad u_2 \quad u_3 \quad u_4]^{\mathrm{T}}$ is the input torque vector of the four reaction wheels. The attitude dynamic equation of

the operation robot is obtained as:

$$\dot{\boldsymbol{h}}_b + \dot{\boldsymbol{h}}_w = \boldsymbol{T}_t \tag{26}$$

where:

$$\boldsymbol{h}_b = \boldsymbol{I}^c \boldsymbol{\omega}_c \tag{27}$$

$$\boldsymbol{h}_w = \boldsymbol{N}\boldsymbol{J}^w \boldsymbol{N}^{\mathrm{T}} \boldsymbol{\omega}_c + \boldsymbol{N}\boldsymbol{J}^w \boldsymbol{\Omega} \tag{28}$$

$$\boldsymbol{T}_w = \boldsymbol{N}\boldsymbol{U} = \boldsymbol{N}(-\boldsymbol{J}^w \dot{\boldsymbol{\Omega}} - \boldsymbol{J}^w \boldsymbol{N}^{\mathrm{T}} \dot{\boldsymbol{\omega}}_c) \tag{29}$$

Let $\boldsymbol{\omega}_c^{\times} = \begin{bmatrix} 0 & -\omega_{cz} & \omega_{cy} \\ \omega_{cz} & 0 & -\omega_{cx} \\ -\omega_{cy} & \omega_{cx} & 0 \end{bmatrix}$.

Thus, the attitude dynamic equation can also be rewritten as:

$$\boldsymbol{I}^c \dot{\boldsymbol{\omega}}_c + \boldsymbol{\omega}_c^{\times}(\boldsymbol{I}^c \boldsymbol{\omega}_c + \boldsymbol{N}\boldsymbol{J}^w \boldsymbol{N}^{\mathrm{T}} \boldsymbol{\omega}_c + \boldsymbol{N}\boldsymbol{J}^w \boldsymbol{\Omega}) = \boldsymbol{T}_t + \boldsymbol{T}_w \tag{30}$$

4. Multi-objective Trajectory Optimization Model Based on Velocity Impulse

The task of TSR is capturing and repairing the uncontrolled satellite. The operation robot should firstly arrive at the desired position. Therefore, the approach time is important. However, thruster fuel is limited. Therefore, this paper presents a multi-objective optimization model based on velocity impulse, which considers the thruster fuel and the approach time simultaneously.

4.1 The Target Function of the Trajectory Optimization Model

The thruster fuel consumption of the operation robot is selected as the first target function, and the approach time is the second function. To simplify the calculation, the minimum-norm solution (solution of Eq. (23)) of total velocity impulse is considered as the total fuel consumption.

The optimal target function is:

$$\boldsymbol{f}(\boldsymbol{x}) = \begin{bmatrix} f_1(\boldsymbol{x}) & f_2(\boldsymbol{x}) \end{bmatrix}^{\mathrm{T}} \tag{31}$$

The constraint condition is:

$$\boldsymbol{g}(\boldsymbol{x}) = \begin{bmatrix} g_1(\boldsymbol{x}) & g_2(\boldsymbol{x}) \end{bmatrix}^{\mathrm{T}} \le 0 \tag{32}$$

$\boldsymbol{x} = \begin{bmatrix} x_1 & x_2 & \cdots & x_n \end{bmatrix}^{\mathrm{T}}$ are optimization variables in Eqs. (31) and (32). The first target function and the second target functions are expressed by Eqs. (33) and (34), respectively.

$$\min(f_1(\boldsymbol{x})) = \sum_{i=1}^{M} |\Delta \boldsymbol{v}_i| \tag{33}$$

$$\min(f_2(\boldsymbol{x})) = t_f \tag{34}$$

4.2 Trajectory Optimization Variable and Trajectory Constraint Conditions

It is easy to obtain optimization variables $\Delta \boldsymbol{v}_i (i = 1, 2 \ldots M)$ and t_f from the Eqs. (33) and (34). However, the terminal equation constraint is hard to handle because of the selection of the optimization variable $\Delta \boldsymbol{v}_i (i = 1, 2 \ldots M)$. Therefore, $\sigma_i (i = 1, 2 \ldots M)$ are selected as optimization variables instead of $\Delta \boldsymbol{v}_i$. The $\Delta \boldsymbol{v}_i$ can be obtained from Eq. (21) or Eq. (23). The terminal equation constraint is satisfied automatically:

$$\sigma_i = t_i / t_f \qquad \sigma_i \le 1 \tag{35}$$

where t_i is the time of imposing velocity and σ_i is the unitary result of t_i. Therefore, the optimization variables $\boldsymbol{x}$ consist of t_f and $\sigma_i (i = 1, 2 \ldots M)$.

There are limitations, such as velocity amplitude and imposing interval. Therefore, the $|\Delta \boldsymbol{v}_i|$ and t_i should be restricted. In the actual approach process, a series of sensors can give exact information in certain areas of the view angle. Therefore, the view angle of the operation robot can be restricted, as shown in Figure 3.

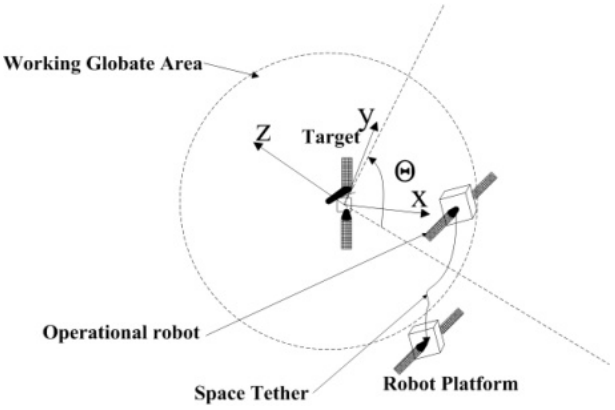

Figure 3. View angle constraint diagram for approaching the target

It is concluded that the constraint conditions of tethered space robot are as follows:

$$t_0 \le t_1 < t_2 \cdots < t_M \le t_f \tag{36}$$

$$t_{i+1} - t_i \ge \Delta t \qquad (i = 1, 2, \ldots M - 1) \tag{37}$$

$$|\Delta \boldsymbol{v}_i| \le |\Delta \boldsymbol{v}|_{\max} \tag{38}$$

$$\theta \le \Theta / 2 \tag{39}$$

where t_i is the time of imposing the velocity impulse by Eqs. (36) and (37). Δt is the minimum time interval and $|\Delta \boldsymbol{v}|_{\max}$ is the maximum velocity impulse by Eq. (37). Θ is the maximum view angle for approaching the target,

$\theta = \mathrm{a}\tan(y/x)$ is the real-time view angle measurement relative to the target by Eq. (38).

4.3 Multi-objective Optimal Trajectory Planning Algorithm

This paper studied optimal trajectory planning for the operation robot after being released from the robot platform. It should be analysed based on a multi-objective velocity impulse, because this process has the characteristics of short approach distance, and fuel and control force limitations.

The aim of multi-objective optimization is to seek Pareto optimal solution sets based on balanced solutions for every target function. The non-dominated sorting genetic algorithm (NSGA) is one of the common methods. However, the drawbacks are obvious, such as the high computational complexity of $O(MN^3)$ (where M is the number of objectives and N is the population size) and lack of advantages. An improved version of NSGA (NSGA-2) adopted a strategy of more available recording, decreasing the total computation time and complexity of $O(MN^2)$, which resulted in better performance than NSGA [25, 26]. This paper studied the multi-objective optimal trajectory planning of the operational robot based on NSGA-2.

5. TSR Coordinated Control for Tracking Optimal Trajectory

The optimal trajectory and ideal velocity impulse have been obtained. First, the characteristics of ideal velocity impulse (amplitude, direction and imposed time) are analysed. Then, the coordinated control law is designed based on errors between the real-time relative position and the ideal trajectory. To save thruster fuel, this control method utilizes the tension force of space tether, thrusters, operation robot and reaction wheel. This paper ignores electricity consumption because the electricity is supplied from the robot platform. The control diagram is shown in Figure 4.

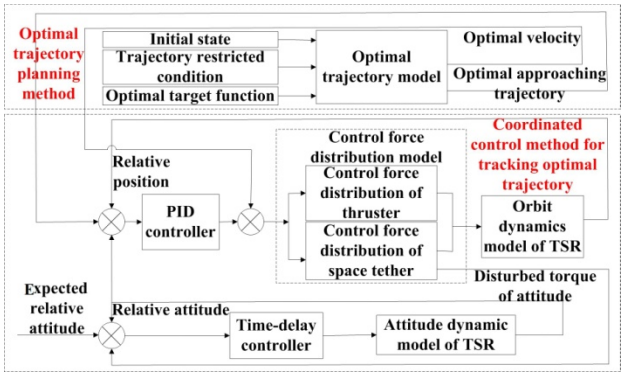

Figure 4. The coordinated controller of tethered space robot

5.1 PID Controller for Tracking Trajectory

The ideal velocity impulse ($\Delta \boldsymbol{v}_i (i = 1, 2 \ldots M)$) is obtained from the ideal optimal approach trajectory. To simplify design of the controller, the $\Delta \boldsymbol{v}_i$ are transformed to constant thrust force $\boldsymbol{F}_i'$ in $o_t x_t y_t z_t$ coordinate frame, t_j is the imposed time of $\Delta \boldsymbol{v}_i$ and t_i is durative time of $\boldsymbol{F}_i'$; we select the t_i as a small number. Therefore, these variables have relationships which are shown by Eq. (40). $\boldsymbol{F}_i'$ should be imposed in period of $[t_j - \frac{t_i}{2}, t_j + \frac{t_i}{2}]$. In addition, the constant thruster force $\boldsymbol{F}_i$ in $o_1 x_2 y_2 z_2$ coordinate frame can be easily obtained from $\boldsymbol{F}_i'$ through Eq. (41). The PID controller can decrease the error between actual position and ideal trajectory. The PID controller is designed by Eq. (42), where, $\boldsymbol{e}$ is the position error, k_P, k_I and k_D are corresponding coefficients, and $\boldsymbol{u}$ is the control vector in $o_1 x_2 y_2 z_2$ coordinate frame.

$$\boldsymbol{F}_i' \cdot t_i = \Delta \boldsymbol{v}_i \tag{40}$$

$$\boldsymbol{F}_i = \begin{bmatrix} -\cos\phi\sin\theta & \cos\phi\cos\theta & \sin\phi \\ -\cos\theta & -\sin\theta & 0 \\ \sin\phi\sin\theta & -\sin\phi\cos\theta & \cos\phi \end{bmatrix} \boldsymbol{F}_i' \tag{41}$$

$$\begin{aligned} \boldsymbol{u}(k) = \boldsymbol{u}(k-1) + k_P[\boldsymbol{e}(k) - \boldsymbol{e}(k-1)] + k_I \boldsymbol{e}(k) + \\ k_D(\boldsymbol{e}(k) - 2\boldsymbol{e}(k-1) + \boldsymbol{e}(k-2)) \end{aligned} \tag{42}$$

5.2 Optimization and Distribution of Tracking Control Force

The purpose of this part is to optimize and distribute the control force to the space tether and thrusters, but the tethered space robot is very complex for the special characteristics of space tether. So simple assumptions are given as follows:

(1) Space tether is massless and inextensible.
(2) Tension force is supplied by releasing or retrieving tether from the rolling motor.
(3) The tether should supply tension force along a straight line for connecting the robot platform and operation robot.
(4) The tether's influence on the robot platform is ignored.

The coordinated control scheme of the operation robot is shown in Figure 5. $O_t x_t y_t z_t$ is the target orbit frame, $\boldsymbol{O_t O_m}$ is the projection vector in $O_t x_t y_t$ plane for the position vector of the operation robot in $O_t x_t y_t z_t$ frame, $\boldsymbol{O_t O_w}$ is the projection vector in $O_t x_t y_t$ plane for the

position vector of the robot platform in $O_t x_t y_t z_t$ frame, $\boldsymbol{O_m O_w}$ is the projection vector in $O_t x_t y_t$ plane of the vector at which the operation robot points to the robot platform in $O_t x_t y_t z_t$ (the angle is α between $\boldsymbol{O_m O_w}$ and the tether's direction), and β is the angle between $\boldsymbol{O_m O_w}$ and $\boldsymbol{O_t O}$, so that:

$$\boldsymbol{O_m O_w} = \boldsymbol{O_t O_w} - \boldsymbol{O_t O_m} \tag{43}$$

F_x, F_y and F_z are the control force of the PID controller in $o_t x_t y_t z_t$ frame. Assume F_t is the tension force of space tether after distributing control force. Meanwhile, F_{xs}, F_{ys} and F_{zs} are the distribution control force of thrusters in $x_t / y_t / z_t$ three directions, so it can be concluded that:

$$F_{xs} = F_x - F_t \cos\alpha \sin\beta \tag{44}$$

$$F_{ys} = F_y + F_t \sin\alpha \cos\beta \tag{45}$$

$$F_{zs} = F_z + F_t \sin\alpha \tag{46}$$

The unit vector of tether direction is obtained according to the geometric relationship:

$$\begin{bmatrix} i_x & i_y & i_z \end{bmatrix}^{\mathrm{T}} = \frac{\boldsymbol{O_m O_w}}{|\boldsymbol{O_m O_w}|} \tag{47}$$

$$\tan\beta = \frac{i_x}{i_y} \tag{48}$$

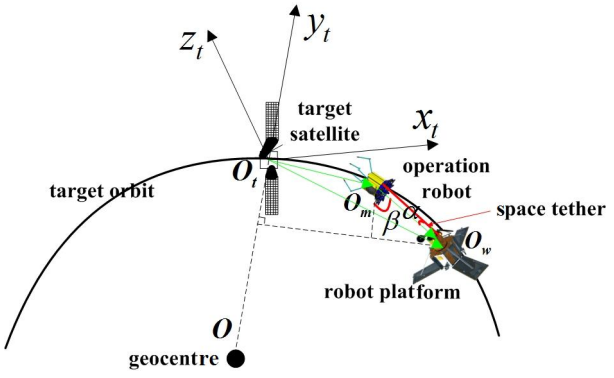

Figure 5. The coordinated control of the operation robot

According to the actual situation of the operation robot for approaching the target, the out-of-plane (z_t direction) motion is ignored. So the cost function of control force optimization and distribution is selected as follows:

$$J_f = w_1 F_{xs} + w_2 F_{ys} \tag{49}$$

where w_1 and w_2 are weight coefficient. It can minimize the cost function while distributing the control force to space tether and thrusters. The weight coefficients w_1 and w_2 are decided by the release direction of the operation robot. If the operation robot is released in the x_t -axis direction, $0 < w_2 < w_1 < 1$. If the operation robot is released in the y_t -axis direction, $0 < w_1 < w_2 < 1$. The primary methods include genetic algorithm [27-29], ant colony algorithm [30] and simulated annealing algorithm [31-32]. The simulated annealing algorithm is adopted for control force optimization and distribution in this article. The control force is optimized and distributed in discrete time points, and the continuous distribution of control force is achieved through polynomial fitting because of the low optimization speed of the simulated annealing algorithm.

The simulated annealing algorithm is derived from the solid annealing principle based on the Monte Carlo iterative method for heuristic searching, and has proved to be in theory a convergence for global optimization. Its control parameters include initial temperature T_0, minimum temperature T_{min}, iteration number n, annealing coefficient ξ and stopping condition. The flow of the simulated annealing algorithm can be described as follows.

Step 1: Initialization. Give the initially guessed solution x_0 (x_0 is the initial tension force of space tether) and the initial temperature T_0, and select the neighbourhood search function. Calculate $J_f(x_0)$, order $x = x_0$, $x_{\min} = x_0$, $J_{f(\min)} = J_f(x_0)$, $i = 0$ (inner loop index) and $j = 0$ (outer loop index).

Step 2: Produce tentative solution. Produce tentative solution $y_i = x_i + \Delta x_i$, where Δx_i is the disturbance to the current solution produced by the neighbourhood search function. The neighbourhood search function is $\Delta x_i = h \times (x_{i(\max)} - x_{i(\min)})$, where h is a random number from a uniform distribution between 0 and 1, $x_{i(\max)}$ and $x_{i(\min)}$ are the upper bound and lower bound of the ith design variable.

Step 3: New solution accepted. First, produce h, between 0 and 1. Then, calculate the probability of accepting the tentative solution y_i based on the current solution x_i and the current temperature T_j.

$$P(y_i \mid x_i, T_j) = \exp\left(\frac{J_f(x_i) - J_f(y_i)}{T_j}\right) \tag{50}$$

If $h \le P(y_i \mid x_i, T_j)$, order $x_{i+1} = y_i$, $J_f(x_{i+1}) = J_f(y_i)$. Otherwise, order $x_{i+1} = x_i$, $J_f(x_{i+1}) = J_f(x_i)$.

Step 4: Judgement. If $J_f(x_{i+1}) < J_{f(\min)}$, order $x_{\min} = x_{i+1}$, $J_{f(\min)} = J_f(x_{i+1})$.

Step 5: Judge Metropolis sampling stabilization rule:

If the Metropolis sampling stabilization rule is satisfied, order $i = 0$, go to step 6. Otherwise, order $i = i + 1$, go to step 2.

The Metropolis sampling stabilization rule is used to determine the number of tentative solutions at the given temperature. A fixed step number *n* is chosen as the inner loop termination rule at the given temperature; the inner loop is terminated, and the temperature is reduced.

Step 6: Judge iteration termination rule. If the iteration termination rule is satisfied, the program terminates; $x_{\min}$ is the near-optimal solution, $J_{f(\min)}$ is the corresponding optimal objective. Otherwise, go to step 7. The iteration termination rule: $T_{\min}$ is chosen as the minimum temperature; if $T_j \le T_{\min}$, the outer loop is ended.

Step 7: Change temperature. According to the given cooling schedule, produce the new temperature T_{j+1} , order $j = j + 1$, go to step 2.

The cooling schedule is taken as $T_{j+1} = \xi T_j$, where ξ is an annealing coefficient.

5.3 Attitude Stability Strategy

The relative attitude interferential torque will be produced when the space tether exerts tension force to the operation robot. Therefore, the attitude stability is an important aspect of the coordinated control method. This article intends to control and stabilize the relative attitude using the time-delay algorithm through the reaction wheels of the operation robot.

The time-delay control method is mainly for dealing with unknown dynamics, such as uncertainties and disturbances without any explicit estimation [33]. The unknown dynamics contain model changes due to external interference. The idea of this method is to supply former period control, compensating the control changes due to the tether's torque interference.

The attitude dynamic equation of the operation robot is given by Eq. (30), where the interferential torque $\boldsymbol{T}_t$ inevitably leads to change in the attitude dynamic model. Therefore, it can utilize control torque to compensate the interference. This section will design a time-delay controller. Eq. (30) can be drawn equivalently:

$$\begin{aligned} &\boldsymbol{I}^c \dot{\boldsymbol{\omega}}_c = -\boldsymbol{\omega}_c^{\times}(\boldsymbol{I}^c \boldsymbol{\omega}_c + \boldsymbol{N}\boldsymbol{J}^w \boldsymbol{N}^{\mathrm{T}} \boldsymbol{\omega}_c + \boldsymbol{N}\boldsymbol{J}^w \boldsymbol{\Omega}) + \\ &\boldsymbol{T}_t + \boldsymbol{N}\boldsymbol{U} + \boldsymbol{Y} \end{aligned} \tag{51}$$

where the control compensation is $\boldsymbol{Y}$, which is uncertain and will be estimated by the former period control. The estimation is $\hat{\boldsymbol{Y}}$. Therefore, Eq. (51) can be drawn:

$$\begin{aligned} &\boldsymbol{Y} \approx \hat{\boldsymbol{Y}} = \boldsymbol{Y}(t-T) = \boldsymbol{I}^c \dot{\boldsymbol{\omega}}_c(t-T) + \boldsymbol{\omega}_c^{\times}(t-T)[\boldsymbol{I}^c \boldsymbol{\omega}_c(t-T) + \\ &\boldsymbol{N}\boldsymbol{J}^w \boldsymbol{N}^{\mathrm{T}} \boldsymbol{\omega}_c(t-T) + \boldsymbol{N}\boldsymbol{J}^w \boldsymbol{\Omega}(t-T)] - \boldsymbol{T}_t - \boldsymbol{N}\boldsymbol{U}(t-T) \end{aligned} \tag{52}$$

Eq. (30) can also be drawn:

$$\boldsymbol{U} = \boldsymbol{N}^{-}[\boldsymbol{I}^c \dot{\boldsymbol{\omega}}_c + \boldsymbol{\omega}_c^{\times}(\boldsymbol{I}^c \boldsymbol{\omega}_c + \boldsymbol{N}\boldsymbol{J}^w \boldsymbol{N}^{\mathrm{T}} \boldsymbol{\omega}_c + \boldsymbol{N}\boldsymbol{J}^w \boldsymbol{\Omega}) - \boldsymbol{T}_t - \boldsymbol{Y}] \tag{53}$$

where $\boldsymbol{N}^{-} = \boldsymbol{N}^{\mathrm{T}}(\boldsymbol{N}\boldsymbol{N}^{\mathrm{T}})^{-1}$ is the Moore-Penrose inverse matrix. Combining Eqs. (52) and (53) gives:

$$\begin{aligned} &\boldsymbol{U} = \boldsymbol{U}(t-T) + \boldsymbol{N}^{+}\boldsymbol{I}^c[\dot{\boldsymbol{\omega}}_c(t) - \dot{\boldsymbol{\omega}}_c(t-T)] + \\ &\boldsymbol{N}^{-}\left\{\boldsymbol{\omega}_c^{\times}(t)[\boldsymbol{I}^c \boldsymbol{\omega}_c(t) + \boldsymbol{N}\boldsymbol{J}^w \boldsymbol{N}^{\mathrm{T}} \boldsymbol{\omega}_c(t) + \boldsymbol{N}\boldsymbol{J}^w \boldsymbol{\Omega}(t)] - \right. \\ &\left. \boldsymbol{\omega}_c^{\times}(t-T)[\boldsymbol{I}^c \boldsymbol{\omega}_c(t-T) + \boldsymbol{N}\boldsymbol{J}^w \boldsymbol{N}^{\mathrm{T}} \boldsymbol{\omega}_c(t-T) + \boldsymbol{N}\boldsymbol{J}^w \boldsymbol{\Omega}(t-T)]\right\} \end{aligned} \tag{54}$$

Eq. (25) shows the relationship between $\boldsymbol{\omega}_r$ and $\boldsymbol{\omega}_c$. In order to satisfy $\boldsymbol{Q}_r \to \boldsymbol{Q}_{rd}$ and $\boldsymbol{\omega}_r \to \boldsymbol{\omega}_{rd}$, the relative attitude and angular velocity are given by:

$$\begin{cases} \boldsymbol{Q}_{rd} = \boldsymbol{Q}_r + t_1 \dot{\boldsymbol{Q}}_r \\ \boldsymbol{\omega}_{rd} = \boldsymbol{\omega}_r + t_2 \dot{\boldsymbol{\omega}}_r \end{cases}, (t_1 > t_2 > 0) \tag{55}$$

Where t_1 and t_2 are time constants, those constants express hanging velocity. It is possible to determine that $t_1 > t_2 > 0$, which means that the angular velocity changed faster than the relative attitude.

The relationship between $\boldsymbol{\omega}_r$ and $\boldsymbol{Q}$ can be expressed by the attitude kinematic equation:

$$\dot{\boldsymbol{Q}}_r = \frac{1}{2}\boldsymbol{Q}_r^{\times}\boldsymbol{\omega}_r \Rightarrow \boldsymbol{\omega}_r = 2(\boldsymbol{Q}_r^{\times})^{-}\dot{\boldsymbol{Q}}_r \tag{56}$$

where $(\boldsymbol{Q}_r^{\times})^{-} = (\boldsymbol{Q}_r^{\times})^{\mathrm{T}}[(\boldsymbol{Q}_r^{\times})(\boldsymbol{Q}_r^{\times})^{\mathrm{T}}]^{-1}$ is an arbitrary, generalized inverse matrix of $\boldsymbol{Q}_r^{\times}$. It is possible to obtain the relationship between $\dot{\boldsymbol{\omega}}_r$ and $\boldsymbol{Q}_r$ by combining Eqs. (55) and (56). The Eq. (25) can be drawn:

$$\dot{\boldsymbol{\omega}}_r = \dot{\boldsymbol{\omega}}_c - \boldsymbol{H}\dot{\boldsymbol{\omega}}_t - (\frac{d\boldsymbol{H}}{dt})\boldsymbol{\omega}_t \Rightarrow \dot{\boldsymbol{\omega}}_r = \dot{\boldsymbol{\omega}}_c + \boldsymbol{\omega}_r^{\times}\boldsymbol{\omega}_c \quad (57)$$

Combining Eqs. (54), (56) and (57), the final time-delay attitude coordinated control law is:

$$\begin{aligned}\boldsymbol{U} &= \boldsymbol{U}(t-T) + \boldsymbol{N}^{-}\boldsymbol{I}^{c}\left[\begin{array}{c} 2(\boldsymbol{Q}_r^{\times})\cdot\dfrac{\boldsymbol{Q}_{rd}-\boldsymbol{Q}_r}{t_1} - \boldsymbol{\omega}_r \\ \dfrac{}{t_2} - \boldsymbol{\omega}_r^{\times}\boldsymbol{\omega}_c - \dot{\boldsymbol{\omega}}_c(t-T) \end{array}\right] \\ &+\boldsymbol{N}^{-}\left\{\boldsymbol{\omega}_c^{\times}(t)[\boldsymbol{I}^{c}\boldsymbol{\omega}_c(t) + \boldsymbol{N}\boldsymbol{J}^{w}\boldsymbol{N}^{\mathrm{T}}\boldsymbol{\omega}_c(t) + \boldsymbol{N}\boldsymbol{J}^{w}\boldsymbol{\Omega}(t)]\right. \\ &\left.-\boldsymbol{\omega}_c^{\times}(t-T)[\boldsymbol{I}^{c}\boldsymbol{\omega}_c(t-T) + \boldsymbol{N}\boldsymbol{J}^{w}\boldsymbol{N}^{\mathrm{T}}\boldsymbol{\omega}_c(t-T) + \boldsymbol{N}\boldsymbol{J}^{w}\boldsymbol{\Omega}(t-T)]\right\}\end{aligned} \quad (58)$$

where $\boldsymbol{Q}_r$, $\boldsymbol{\omega}_r$ and $\boldsymbol{\omega}_c$ can be obtained by relative sensors, and the $\dot{\boldsymbol{\omega}}_c(t-T)$ can be estimated by:

$$\dot{\boldsymbol{\omega}}_c(t-T) = \frac{\boldsymbol{\omega}_c(t-T) - \boldsymbol{\omega}_c(t-2T)}{T} \quad (59)$$

The interferential torque is related to tension force, the connection point between the tether and the operation robot. Assume the distances between the connection point and the centroid of the operation robot are l_x , l_y and l_z . The interferential torque $\boldsymbol{T}_t$ can be estimated by Eq. (60).

$$\boldsymbol{T}_t = \boldsymbol{l}^{\times}\boldsymbol{F}_t, where \quad \boldsymbol{l}^{\times} = \begin{bmatrix} 0 & -l_z & l_y \\ l_z & 0 & -l_x \\ -l_y & l_x & 0 \end{bmatrix} \quad (60)$$

6. Examples and Numerical Results

6.1 Initial Conditions

Assume: the operation robot is approximately 10 kg, the robot platform is about 2000 kg; l_x = 0.3 m; l_y = 0.3 m; and l_z = 0 m. $\boldsymbol{X}_0$ denotes the initial states and $\boldsymbol{X}_f$ is the final desired position.

$\boldsymbol{X}_0 = (139.63\text{m} \quad -0.0012\text{m} \quad 0\text{m} \quad -1.5\text{m/s} \quad 0\text{m/s} \quad 0\text{m/s})^{\mathrm{T}}$, $\boldsymbol{X}_f = (0 \quad 0 \quad 0 \quad 0 \quad 0 \quad 0)^{\mathrm{T}}$. $\boldsymbol{Q}_{r0}$ is the initial relative attitude of the operation robot and $\boldsymbol{Q}_d$ is the desired relative attitude. $\boldsymbol{Q}_{r0} = [1 \quad 0 \quad 0 \quad 0]^{\mathrm{T}}$ and $\boldsymbol{Q}_d = [1 \quad 0 \quad 0 \quad 0]^{\mathrm{T}}$, $\boldsymbol{N} = \begin{bmatrix} 1 & 0 & 0 & 1 \\ 0 & 1 & 0 & 1 \\ 0 & 0 & 1 & 1 \end{bmatrix}$. The mass of the reaction wheel is 0.2 kg. The simulation parameters for trajectory planning are shown in Table 1. The other relevant parameters for the coordinated control method are shown in Table 2.

Type of parameter	Value	Type of parameter	Value
The maximum value of velocity	1 m/s	Time of fight t_f	100 s~ 500 s
The maximum number of generations	200	$\sigma_i (i = 1, 2 \ldots M)$	0~1
Population size	100	Δt	50 s
Number of velocity impulse	2, 3, 4	θ	±90°

Table 1. Simulation parameters for trajectory planning

Model parameters	$\boldsymbol{I}^{c} = \begin{bmatrix} 3 & -3.5e{-}3 & -1.5e{-}4 \\ -3.5e{-}3 & 1.5 & -4.6e{-}4 \\ -1.5e{-}4 & -4.6e{-}4 & 1.8 \end{bmatrix}$ kg·m²	$\boldsymbol{J}^{w} = \begin{bmatrix} 0.01 & 0 & 0 & 0 \\ 0 & 0.01 & 0 & 0 \\ 0 & 0 & 0.01 & 0 \\ 0 & 0 & 0 & 0.01 \end{bmatrix}$ kg·m²
Target orbi parameters	Orbit altitude h = 1622km, Argument of perigee w =40°	True anomaly f_t =0.001°
Robot platform orbit parameters	Orbit inclination i = 30 deg, Eccentricity $e = 0$ Longitude ascending node Ω_0 =10 deg	True anomaly f_c =0°
Optimizatio n parameters	T_0 =100	T_{min} =0.01
	n =500	ξ =0.85
	$w_1 = 0.8$, $w_2 = 0.2$	

Table 2. Other relevant parameters for coordinated control

6.2 Simulation for Optimal Trajectory Planning of Operation Robot

The operation robot has two and three velocity impulses imposed separately using NSGA-2 optimization algorithm, and the approaching time is 100 s ~ 300 s, which are estimated by relative distance and velocity at the initial time. Figure 6 shows the Pareto optimal solution set; the abscissa expresses the flight time and the y-axis expresses fuel consumption (total velocity impulse). One hundred optimal solutions are obtained from every simulation condition (two and three velocity impulses). We can see that the optimal solutions of flight time are concentrated between 100 s and 190 s in two-velocity impulse mode; otherwise, the optimal solutions of flight time are concentrated between 100 s and 300 s in three-impulse mode. The relationship between approach time and fuel consumption is one of inverse proportion. The operation robot consumes more fuel in three-velocity impulse mode than in two-velocity mode in the same flight time.

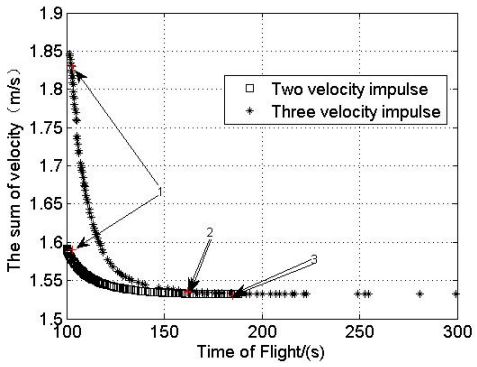

Figure 6. Pareto optimal sets

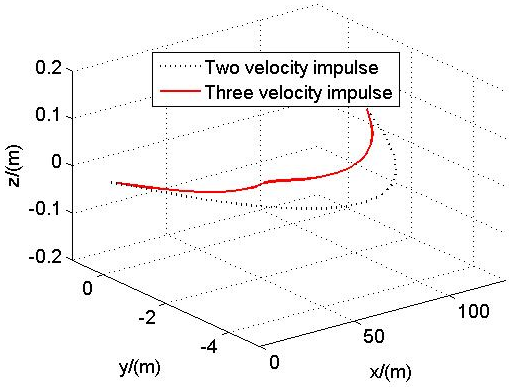

(a) Relative track curve between 0 s and 103 s

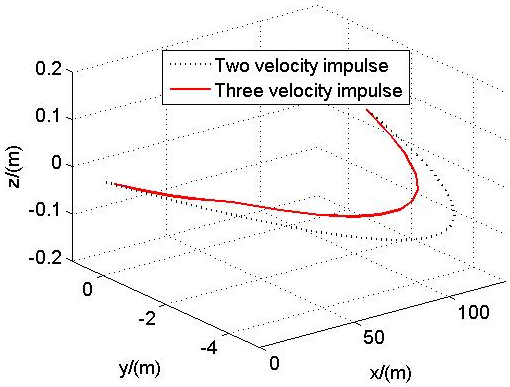

(b) Relative track curve between 0 s and 162 s

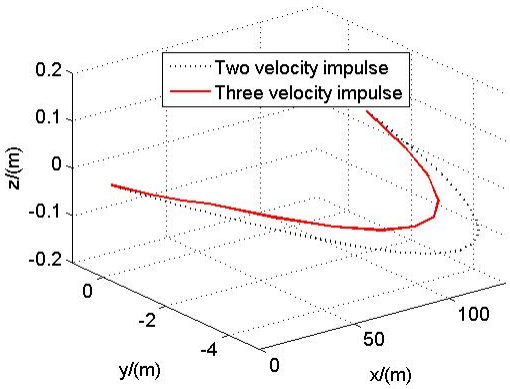

(c) Relative track curve between 0 s and 185 s

Figure 7. The relative track of two modes for TSR

We select position "1" at 103 s; position "2" at 162 s; and position "3" at 185 s from Figure 6. Figure 7 shows the relative trajectory of the operation robot based on the two modes. The relative trajectories at different approach times are similar. However, the movement trend in the y-axis direction (radial direction) in three-velocity impulse mode is much less than the x-axis movement in two-velocity impulse mode. Following increase in flight time, the movement trend in the y-axis direction becomes larger. The out-of-plane movement is nearly zero and can be ignored.

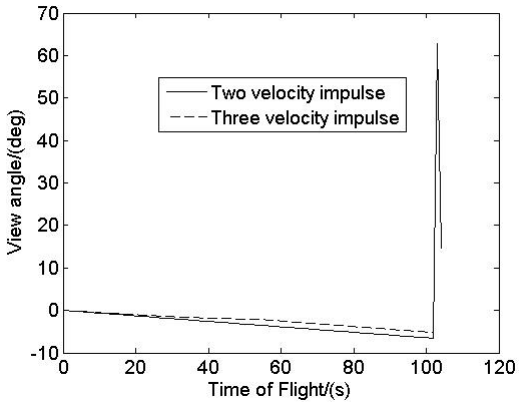

(a) Relative view angle curve between 0 s and 103 s

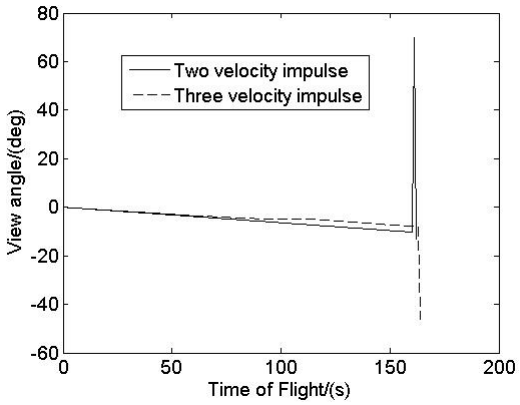

(b) Relative view angle curve between 0 s and 162 s

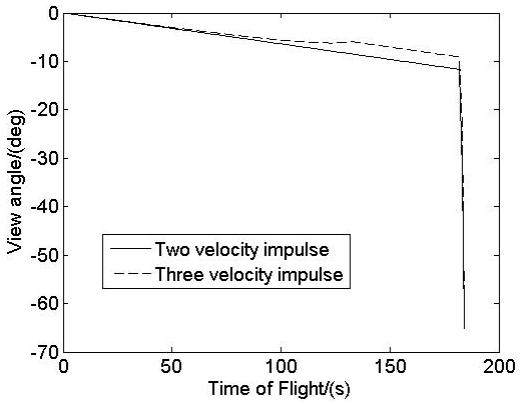

(c) Relative view angle curve between 0 s and 185 s

Figure 8. The view angle curves of two modes for TSR

This paper ignores the out-of-plane view angle because the movement trend in the z-axis is less obvious than in the other two directions. Figure 8 shows the view angle curve of the operation robot based on the two velocity impulse modes. The view angle curve is similar, with two modes at position "1", "2" or "3". The view angle will decrease with the increase number of velocity impulses, which is useful for the working of relative sensors.

From the above simulation, it can be seen that the NSGA-2 optimization algorithm is useful for trajectory planning based on velocity impulse of TSR. The fuel consumption is always contrary to the approach time. However, the fuel consumption is not contrary to the relative view angle. Therefore, the optimal trajectory can be selected from the Pareto optimal solution set according to special task requirements. The amplitude of velocity will decrease when the approach time increases. The in-plane view angle will decrease when the number of velocity impulses increases, which is useful for the relative sensors.

6.3 Simulation of Coordinated Control Method for Tracking Optimal Trajectory

This paper presents a coordinated control method using thrusters, space tether and reaction wheels in the process of tracking the optimal trajectory. Taking the optimal trajectory of two-velocity impulse mode as an example, its approach time is 162 s. The ideal velocity impulses are 0.6439/-0.1565/0 (m/s) in $t_0 = 0$ and 0.856/-0.1565/0 (m/s) in $t_f = 162$ s. This velocity impulse can be transformed to standard control force by Eqs. (40) and (41). However, the error between velocity impulse and standard control force exists, and there is a measurement error and other errors. Therefore, the PID controller should be designed. It is assumed that the real-time position measurement r_{rel} is $r \pm 0.05r$ (r is the true position). All the control force can be expressed in the $o_t x_t y_t z_t$ frame in order to illustrate the effect on saving the thruster fuel using space tether.

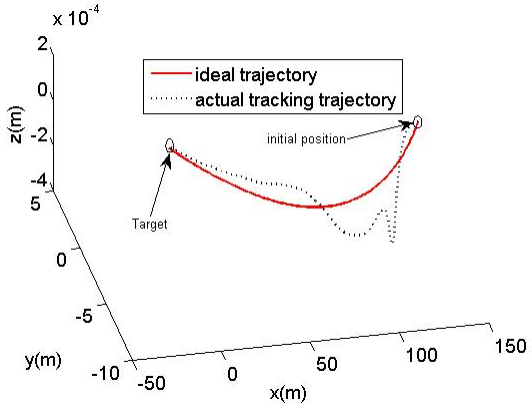

Figure 9. Comparison between ideal trajectory and tracking trajectory

Figure 9 shows the comparison between ideal trajectory and tracking trajectory. The operation robot can track the optimal approach trajectory effectively using this coordinated control method. Figure 10 shows the states of the space tether. The states contain in-plane angle, out-of-plane angle and releasing length. The out-of-plane angle ϕ is nearly zero because of reduced out-of-plane movement. The in-plane angle θ starts from 90° and moves to 79°, which can reveal the approach characteristics of the operation robot in this numerical example. The states of the space tether can express the approach trajectory of the operation robot in another way.

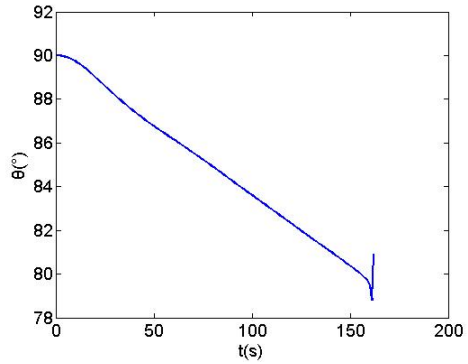

(a) In-plane angle of space tether

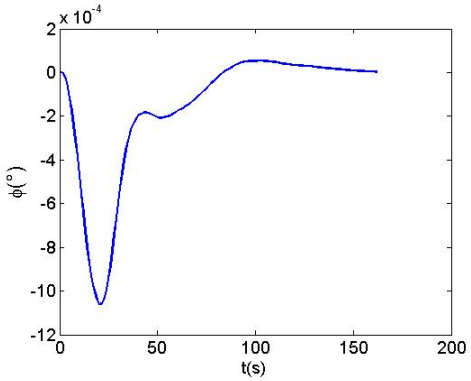

(b) Out-of-plane angle of space tether

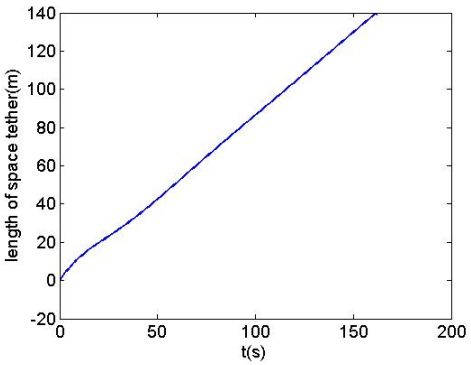

(c) Releasing length of space tether

Figure 10. The states of space tether

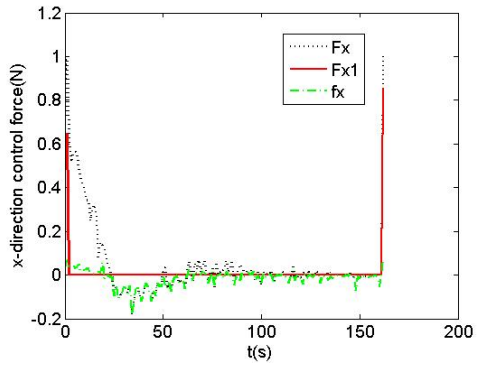

(a) The control force comparison in x-direction

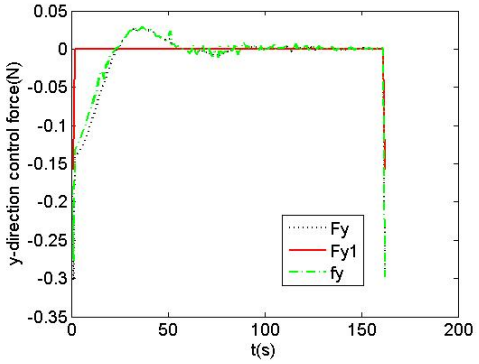

(b) The control force comparison in y-direction

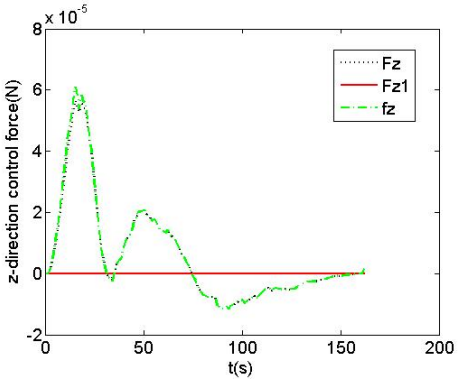

(c) The control force comparison in z-direction

Figure 11. Thruster force comparison between single PID control and coordinated control

Figure 11 shows a thruster force comparison between single PID control and coordinated control. Fx, Fy and Fz are thruster control force in the x_t - axis, y_t - axis and z_t - axis directions, respectively, using a single PID controller. Fx1, Fy1 and Fz1 are transformed standard thruster control force from an ideal velocity impulse. fx, fy and fz are the distributed control forces of the thruster using coordinated control method. Fx and Fx1 are different to a certain extent, due to the velocity transformed error, measurement error and other errors, which are the same as in the other two directions. The positive force of fx can be decreased to nearly zero compared with Fx using this coordinated orbit control method. As a result of the releasing mode, the thruster fuel cannot be saved effectively in the other two directions. However, the thruster fuel consumptions of the x_t - axis direction are of primary importance among the total fuel consumptions. Therefore, the thruster fuel can be saved effectively using the coordinated control method. The space tether can only supply tension force, which can be also be seen from the simulations.

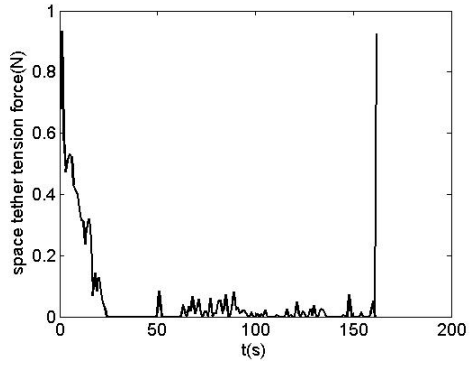

(a) The tether tension force

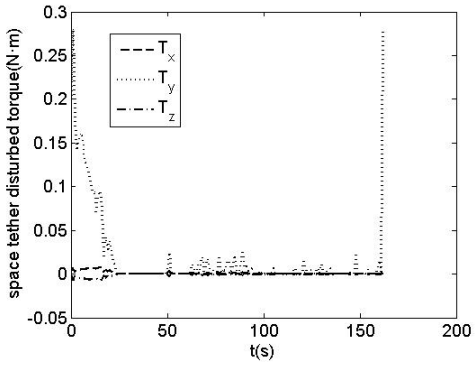

(b) The interference torque of tether tension force

Figure 12. Tethered tension force and its interference torque

Figure 12 shows the tether tension force and the interferential torque produced by the space tether. In the periods of 0 s~30 s and 150 s~162 s, the space tether can supply tension force that can save thruster fuel in the x_t - axis direction. Therefore, the operation robot can be influenced by the interferential attitude torque at the same approach time. The interferential attitude torque remains between -0.3 N·m and +0.3 N·m.

Figure 13a shows the relative attitude angle controlled by reaction wheels using the coordinated attitude control method. At the early stage, the roll angle φ_1, pitch angle θ_1 and yaw angle ψ_1 are held between -2° and 2°. Finally, the relative attitude angles are stabilized between -0.5° and 0.5°, which can satisfy the attitude requirement. Figure 13b shows the relative angular velocity of the operation robot. The results show that relative angular velocity is maintained at less than 0.015 rad/s after using the coordinated attitude control method, which satisfies the stability requirement.

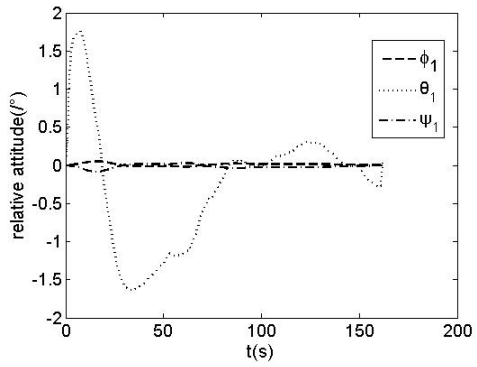

(a) The relative attitude

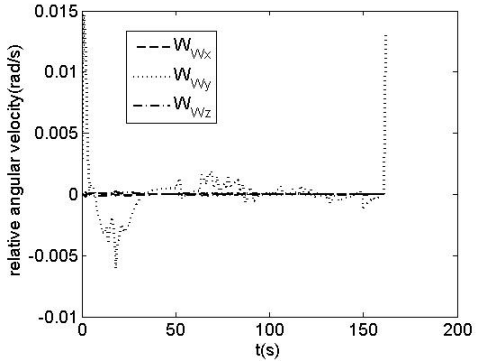

(b) The relative angular velocity

Figure 13. The relative attitude and relative angular velocity for tethered space robot

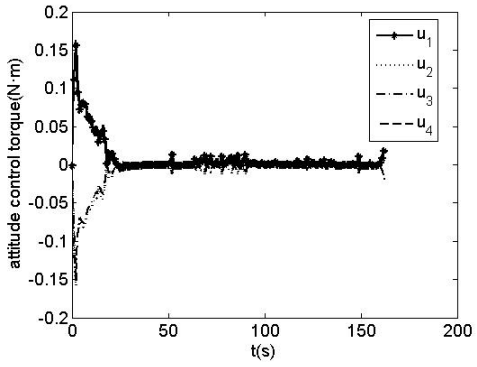

(a) The attitude control torque of reaction wheel

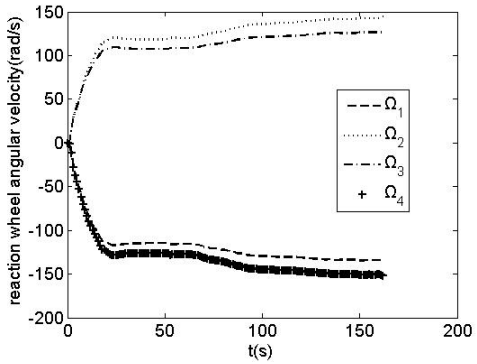

(b) The angular velocity of reaction wheel

Figure 14. The attitude control torque and angular velocity of reaction wheel

The attitude control torque is shown in Figure 14a, the angular velocity of the reaction wheels are shown in Figure 14b. The reaction wheels are stable after 30 s. The corresponding attitude control torque is supplied by reaction wheels before 30 s. Hence, the robot's attitude can be stabilized between 0 s and 100 s.

In this simulation, we select the same special circular orbit for the target and the TSR. If the target orbit and TSR orbit are different, or the target and TSR are located in the same ellipse orbit, the distance between target and robot platform should be measured in real-time with the help of the sensors of the robot platform, which may result in changing the direction of the tether tension force. Furthermore, the y_t -axis or z_t -axis direction thruster fuel may be saved through tether tension force. However, the rule of the simulation results is the same if we transform the above initial conditions.

It can be concluded that the proposed coordinated control method can make the operation robot track the optimal trajectory effectively based on velocity impulses. This transformed optimal velocity impulse can be used to standardize control force, and the PID controller can be designed with consideration for the position measurement error. Then, the control force can be distributed to the space tether and thrusters. The interferential torque produced by the space tether is stabilized using the attitude stability method based on a time-delay algorithm through reaction wheels in the interim.

7. Conclusions

First, this paper studies a multi-objective optimal trajectory planning method based on velocity impulses using an NSGA-2 algorithm. Then, the article proposes a coordinated control method for tracking the optimal trajectory. For optimal trajectory planning, the optimal Pareto solution sets are calculated for two- and three-impulse modes in periods of 100 s ~ 300 s. The relative trajectory and view angle of operation robot are simulated at three special positions for two-velocity impulse modes. The simulations show this trajectory planning method can clearly reveal the relationships among fuel consumption, approach time, view angle and imposed number of velocity impulses. A suitable optimal trajectory can be selected according to special task requirements. For the coordinated control method, the paper designs the PID controller combined with the transformed standard ideal control force. Thus, the ideal control force is obtained. To save thruster fuel, the ideal control force is optimized and distributed to the space tether and thrusters. The interferential torque of the space tether is stabilized using the attitude stability method based on a time-delay algorithm through the reaction

wheels. Simulation results show this coordinated control method can make the operation robot track the optimal trajectory based on velocity impulse, and maintain relative attitude effectively.

8. Acknowledgments

This work was supported by the National Natural Science Foundation of China (Grant No: 11272256, 61005062) and the Doctorate Foundation of Northwestern Polytechnical University (Grant No: CX201217).

9. References

[1] T.E. Carter, S.A. Alvarez (1998) Four-Impulse Rendezvous Near Circular Orbit. AIAA Journal. j. 1998: 1-19.

[2] O. Abdelkhalik, D. Mortari (2007) N-impulse orbit transfer using genetic algorithms. Journal of Spacecraft and Rockets. j. 44: 456-459.

[3] H.Y. Li, Y.Z. Luo, J. Zhang et al. (2010) Optimal multi-objective linearized impulsive rendezvous under uncertainty. Acta Astronautica. j. 66: 439-445.

[4] M. Vasile, E. Minisci (2010) Analysis of some global optimization algorithms for space trajectory. Journal of Spacecraft and Rockets. j. 47: 334-344.

[5] G. Radice, G. Olmo (2006) Ant colony algorithms for two-impulse interplanetary trajectory optimization. Journal of Guidance, Control, and Dynamics. j. 26: 1440-1443.

[6] Y.Z. Luo, G.J. Tang, H.Y. Li(2006) Optimization of multiple-impulse minimum-time rendezvous with impulse constraints using a hybrid genetic algorithm. Aerospace Science and Technology. j. 10: 534-540.

[7] Y.H. Kim, D.B. Spencer (2002) Optimal spacecraft rendezvous using genetic algorithms. Journal of Spacecraft and Rockets. j. 39: 859-865.

[8] D.W. Zhang, S.M. Song, G.R. Duan (2002) Fuel and time optimal transfer of spacecrafts rendezvous using Lambert's theorem and improved genetic algorithm. IEEE Transactions on Evolutionary Computation.

[9] N. Yuya, S. Fumiki, N. Shinichi (2005) Guidance and control of "tethered retriever" with collaborative tension-thruster control for future on-orbit service missions. The 8th International Symposium on Artificial Intelligence: Robotics and Automation in Space-ISAIRAS, Munich, Germany.

[10] N. Masahiro, D. N. Nenchev, U. Masaru (2001) Tethered robot casting using a spacecraft-mounted manipulator. Journal of Guidance, Control and Dynamics. j. 24: 827-833.

[11] Godard, K. D. Kumar, B. Tan (2008) Fault-tolerant stabilization of a tethered satellite system using offset control. Journal of Spacecraft and Rockets. j. 45: 1070-1084.

[12] N. Masahiro (2004) Attitude control of a tethered space robot by link motion under microgravity. Proceedings of the 2004 IEEE International Conference on Control Applications, Taipei, Taiwan.

[13] M. Osamu, M. Saburo (2001) Coordinated control of tethered satellite cluster systems. AIAA Guidance, Navigation, and Control Conference and Exhibit, Montreal, Canada.

[14] I. Chang, S. J. Chung (2009) Bio-inspired adaptive cooperative control of heterogeneous robotic networks. AIAA Guidance, Navigation, and Control Conference, Chicago, USA.

[15] E. Silani, M. Lovera (2005) Magnetic spacecraft attitude control: A survey and some new results. Control Engineering Practice, InTech, pp. 357-371.

[16] S. S. Nudehi, U. Farooq, A. Alasty, J. Issa (2008) Satellite attitude control using three reaction wheels. American Control Conference Westin Seattle Hotel, Seattle, Washington, USA, 2008.

[17] B. L. Wu, X. B. Cao, Z. G. Li (2009) Multi-objective output-feedback control for microsatellite attitude control: An LMI approach, Acta Astronautica. j. 64 : 1021-1031.

[18] M. Aliabbasi, H. A. Talebi, M. Karrari (2002) A satellite attitude controller using nonlinear H∞ approach. Proceedings of the 41st IEEE Conference on Decision and Control, Las Vegas, Nevada, USA.

[19] S. N. Singh, W. Yim (2005) Nonlinear adaptive spacecraft attitude control using solar radiation pressure. IEEE Transactions on Aerospace and Electronic Systems. j. 41: 770-779.

[20] M. Belanger, J. D. Lafontaine (2006) Quaternion-based satellite attitude control using fuzzy logic. Proceedings of the AAS/AIAA Astrodynamics Specialists Conference, Keystone, Colorado.

[21] F. Nagi, S. K. Ahmed, A. A. Z. Abidin, F. H. Nordin (2010) Fuzzy bang-bang relay controller for satellite attitude control system. Fuzzy Sets and Systems. j. 161: 2104-2125.

[22] R. Kristiansen, O. Egeland, P. Johan (2005) A comparative study of actuator configurations for satellite attitude control. Modeling, Identification and Control. j. 26: 201-219.

[23] Z. Ismail, R. Varatharajoo (2010) A study of reaction wheel configurations for 3-axis satellite attitude control. Advances in Space Research. j. 45: 750-759.

[24] J. Jin, S. Ko, C. K. Ryoo (2008) Fault tolerant control for satellites with four reaction wheels. Control Engineering Practice. j. 16: 1250-1258.

[25] Y.Z. Luo, G.J. Tang, Y.J. Lei (2007) Optimal multi-objective linearized impulsive rendezvous. Journal of Guidance, Control, and Dynamics. j. 30: 383-389.

[26] Y.Z. Luo, Y.J. Lei, G.J. Tang (2007) Optimal multi-objective nonlinear impulsive rendezvous. Journal of Guidance, Control, and Dynamics. j. 30: 994-1002.

[27] K. Deb, A. Pratap, S. Agarwal et al. (2002) A fast and elitist multiobjective genetic algorithm: NSGA-II.

IEEE Transactions on Evolutionary Computation. j. 6: 182-197.
[28] Y. Z. Luo, G. J. Tang, H. Y. Li (2006) Optimization of multiple-impulse minimum-time rendezvous with impulse constraints using a hybrid genetic algorithm. Aerospace Science and Technology. j. 10: 534-540
[29] Z. Michalewicz, C. Z. Janikow, J. B. Krawczyk (1992) A modified genetic algorithm for optimal control problem. Computers & Mathematics with Applications. j. 23:83-94.
[30] R. Gianmarco, O. German (2006) Ant colony algorithms for two-impulse interplanetary trajectory optimization. Journal of Guidance, Control, and Dynamics. j. 26:1440-1443.
[31] Y. Z. Luo, G. J. Tang (2005) Spacecraft optimal rendezvous controller design using simulated annealing. Aerospace Science and Technology. j. 9: 732-737.
[32] T. Motoda, F. S. Robert, M. Yoshikazu (1998) Robust control system using simulated annealing. Journal of Guidance, Control and Dynamics. j. 25:267-274.
[33] K.Y. Toumi, S. Reddy (1992) Analysis of linear time invariant systems with time delay. ASME Journal of Dynamic Systems, Measurement and Control. j. 114: 544-555.